SLAC-PUB-12299
January 2007

Beam test of a prototype phoswich detector assembly for the PoGOLite astronomical soft gamma-ray polarimeter

Y. Kanai [a,*], M. Ueno [a], J. Kataoka [a], M. Arimoto [a], N. Kawai [a], K. Yamamoto [b], T. Mizuno [b], Y. Fukazawa [b], M. Kiss [c], T. Ylinen [c], C. Marini Bettolo [c], P. Carlson [c], W. Klamra [c], M. Pearce [c], P. Chen [d], B. Craig [d], T. Kamae [d], G. Madejski [d], J.S.T. Ng [d], R. Rogers [d], H. Tajima [d], T.S. Thurston [d], Y. Saito [e], T. Takahashi [e], S. Gunji [f], C-I. Bjornsson [g], S. Larsson [g], F. Ryde [g], G. Bogaert [h] and S. Kishimoto [i]

[a] *Tokyo Institute of Technology, 2-12-1 Ookayama, Meguro, Tokyo, 152-8551, Japan*

[b] *Hiroshima University, Higashi-Hiroshima, Japan*

[c] *Royal Institute of Technology, Stockholm, Sweden*

[d] *Stanford Linear Accelerator Center, Menlo Park, CA, USA*

[e] *Institute of Space and Astronautical Science, Japan Aerospace Exploration Agency, Sagamihara, Japan*

[f] *Yamagata University, Yamagata, Japan*

[g] *Stockholm University, Stockholm, Sweden*

[h] *Ecole Polytechnique, Palaiseau, France*

[i] *Institute of Materials Structure Science, High Energy Accelerator Research Organization, Tsukuba, Japan*

Abstract

We report about the beam test on a prototype of the balloon-based astronomical soft gamma-ray polarimeter, PoGOLite (Polarized Gamma-ray Observer - Light Version) conducted at KEK Photon Factory, a synchrotron radiation facility in Japan. The synchrotron beam was set at 30, 50, and 70 keV and its polarization was monitored by a calibrated polarimeter. The goal of the experiment was to validate the flight design of the polarimeter. PoGOLite is designed to measure polarization by detecting a Compton scattering and the subsequent photo-absorption in an array of 217 well-type phoswich detector cells (PDCs). The test setup included a first flight model PDC and a front-end electronics to select and reconstruct valid Compton scattering events. The experiment has verified that the flight PDC can detect recoil

Submitted to Nuclear Instrumentation and Methods (NIM) A

Work supported in part by the US Department of Energy contract DE-AC02-76SF00515

electrons and select valid Compton scattering events down to 30 keV from background. The measure azimuthal modulations (34.4 %, 35.8 % and 37.2 % at 30, 50, and 70 keV, respectively) agreed within 10% (relative) with the predictions by Geant4 implemented with dependence on the initial and final photon polarizations.

Key words: Polarization, Soft gamma-ray, Hard X-ray, Balloon experiment
PACS: 95.55.Q

1 Introduction

Celestial X-ray and gamma-ray sources have been studied using their spectrum, time variability and 2-dimensional projected image. For many sources, such observations alone do not identify the dominant emission mechanism and polarization measurements are expected to yield important additional information. Spectral dependence of polarization helps identifying the emission process and orientation of the polarization plane probes the distributions of magnetic field, radiation field, and matter around the sources. Polarization measurement will be particularly important for study on gamma-ray pulsars, accreting black holes, and jet-dominated active galaxies. Strong X-ray and gamma-ray polarization can arise from synchrotron emission in ordered magnetic fields, photon propagation in extremely strong magnetic fields ($B > 10^{12}$ gauss) and anisotropic Compton scattering [1].

Despite potential importance of polarization measurement, there has been only one significant polarization detection in the X-ray band (2.6 and 5.2 keV) from the Crab nebula with an instrument aboard the OSO-8 satellite [2,3]. Due to its small effective area, the instrument could not detect polarization from the Crab pulsar and other sources [4,5]. In the hard X-ray and gamma-ray band, polarization has not been detected significantly for objects other than the sun. There is a report of polarization detection from a gamma-ray burst with an instrument on the RHESSI satellite in 2002 [6]. This claim has been seriously challenged and hence remains controversial [7,8].

Polarization measurements are known to be most effective in the hard X-ray and soft gamma-ray band where non-thermal processes are expected to produce high degrees of polarization. Two techniques have been developed to measure X-ray or soft gamma-ray polarization from astrophysical sources. Below 10 keV, polarization can be deduced by tracking the electron from photo-absorption in an imaging gas detector. From about 25 keV to a few

* Corresponding author. Tel./fax: +81-3-5734-2388
Email address: kanai@hp.phys.titech.ac.jp (Y. Kanai).

hundred keV, polarization can be determined by measuring the azimuthal angle distribution of Compton scattered photons. To apply the former technique to astronomical observation, an instrument has to be launched into a satellite orbit. Instruments relying on the latter technique can make observation on a high altitude balloon because the atmospheric overburden ($\sim 3-4$ g/cm^2) is transparent in its energy range (> 25 keV). However the large background produced by cosmic-ray particles in this energy band poses big challenge for detector design.

Several instruments are under development to detect X-ray or gamma-ray polarization from astronomical sources on the Compton scattering technique: some are designed for flights on a balloon and other on a satellite. Most instruments set their primary target at gamma-ray bursts including POLAR [9] (E =10−300 keV, satellite) and GRAPE [10] (E =50−300 keV, long-duration balloon or satellite). PHENEX [11] is designed to detect 10 % polarization from Crab nebula in the 40−300 keV range in a 3-hour balloon observation. CIPHER [12] is designed for observing steady objects in the energy range between 10 keV and 1 MeV with capability of detecting 5 % polarization in the Crab nebula in a 3-hour observation on a satellite orbit.

Polarized Gamma-ray Observer - Light Version (PoGOLite) is a balloon-borne astronomical soft gamma-ray polarimeter and measures polarization in the energy range of 25−100 keV by using the azimuthal angle anisotropy of Compton scattered photons. Its design is based on the well-type phoswich technology proven to be very effective in reducing cosmic-ray background through the WELCOME balloon experiment [13–19] and the Suzaku Hard X-ray Detector [20–26]. A maiden balloon flight of PoGOLite is scheduled in 2009.

The instrument (PoGO) was originally designed to record Compton scattering and photo-absorption in an array of 397 phoswich detector cells (PDCs) made of plastic and bismuth germanate oxide (BGO) scintillators, surrounded by active BGO shields [27,28]. Through the detector simulation and design, cost estimation, and prototype testing, we reached the lighter version of the original PoGO design, PoGOLite. The lighter-weight design will allow to reach a higher altitude (42 km with a 1 million m^3 balloon) and the lower energy limit to 25 keV. The lighter design also simplifies implementation of rotating mechanism around its axis, which is essential in reducing systematic errors in polarization measurement. The pointing system and gondola design have been adopted from the flight-proven High Energy Focusing Telescope (HEFT) design [29]. The overall design of the PoGOLite polarimeter and gondola has incorporated features needed to make long duration balloon flights from Sweden to North America.

The PoGOLite detector consists of a hexagonal close-packed array of 217 well-type PDCs and side anti-coincidence detectors (SAS) made of BGO scintil-

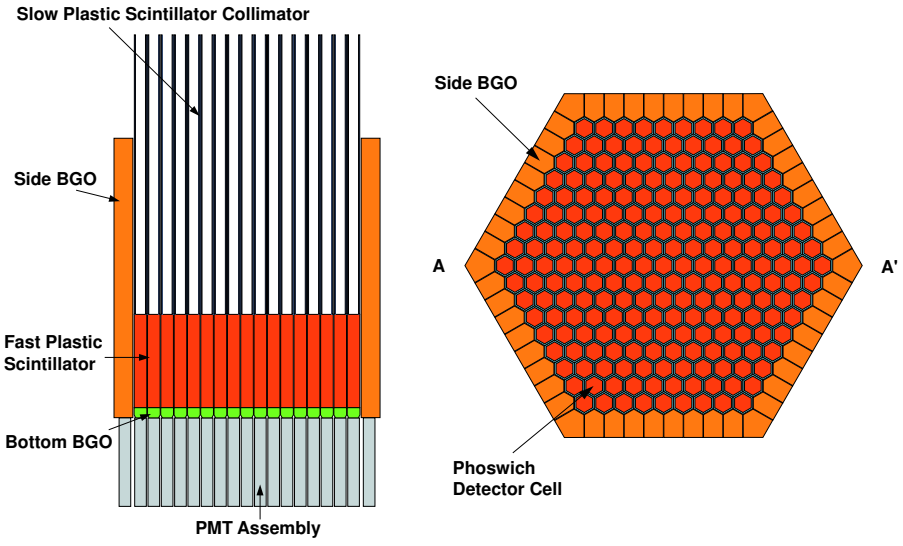

Fig. 1. The PoGOLite detector array. Vertical cross-section AA' (left) and top view (right).

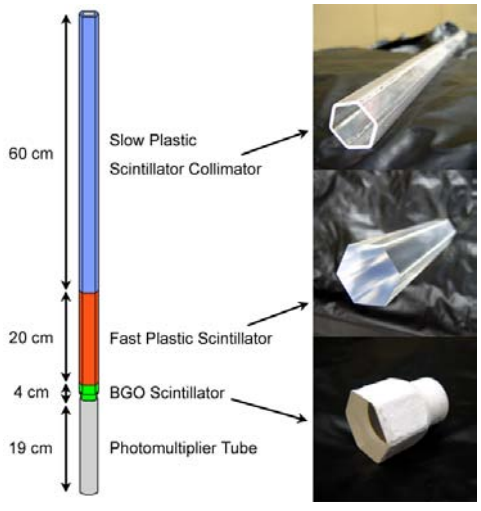

Fig. 2. A schematic view of a PDC and photographs of the component scintillators. The diameter of PMT is 2.6 cm and the width of scintillators is 2.8 cm.

lators, as shown in Fig. 1. Each PDC, as shown in Fig. 2, is composed of a thin-walled tube (well) of slow plastic scintillator at the top (fluorescence decay time 230 ns), a solid rod of fast plastic scintillator (decay time 2 ns), and a BGO crystal at the bottom (Bottom BGO) (decay time 300 ns), all viewed by one photomultiplier tube (PMT). The wells serve as an active collimator, the fast scintillator rods as Compton scatterer and active photon detectors, and the bottom BGOs act as a lower active shield. The energy deposited in a valid Compton scattering event is measured at least two locations in the fast scintillators, at the Compton scattering site and the photo-absorption site. The direction of the scattered photon is deduced from the relative magnitudes of the energy deposited at these locations and the polarization is simply deter-

mined from the distribution of azimuthal scattering angles. Signals from the fast scintillator and those from the slow/BGO scintillator can be discriminated by their temporal profiles (Pulse Shape Discrimination, PSD). In the present beam test, we compared the outputs from two amplifiers with two different shaping times.

Major background sources are cosmic-rays, atmospheric gamma-rays and astronomical gamma-rays. The detector response to the latter two kinds has been studied by Monte Carlo simulation with a background model for the balloon environment [30]. If gamma-rays enter the Compton scatterer from the aperture, they become irreducible background. Gamma-rays can be scattered in the collimator without being detected and hit the Compton scatterer, they also become background. These gamma-rays are reduced by making the aperture narrow ($\sim 2.3 \times 2.3$ deg^2), surrounding the Compton scatterer with thick BGO crystals, and imposing energy depositions compatible with Compton scattering. Background related to charged cosmic-rays is eliminated by the BGO shields and the active collimator embedded in the phoswich cells. Background due to neutrons is reduced to a negligible level by tight Compton kinematics filter. The background rate is expected to be equivalent to about 10 mCrab at 40 keV. With this low background and the large effective area (about 260 cm^2 at 40 keV), PoGOLite is able to detect 10% plane-polarized signal from a 100 mCrab source in a single 6-hour flight.

Prior to the present beam test, we had completed two rounds of prototyping and testing on polarized gamma-ray beams. The first beam test was performed in 2003 at the Advanced Photon Source Facility of the Argonne National Laboratory. The prototype detector was made of 7 fast plastic scintillation counters spaced wider than the flight model design. The azimuth modulation was measured at beam energies of 60, 73 and 83 keV. The analysis led to finding errors in the treatment of photon polarization in Compton/Rayleigh scattering in Geant4 [31]. In 2004, a second experiment was conducted at the Photon Factory of High Energy Accelerator Research Organization (KEK-PF) in Japan. In this experiment, 7 fast plastic scintillation counters were laid out identical to the flight model design. The test covered the lower energy range (30−70 keV) [32].

The goals of the present beam test are:

- Measure the modulation factor and the detection efficiency accurately with a flight model phoswich detector cell in the lower energies;
- Establish effective background filtering procedure;
- Make a quantitative comparison between the measured detector performance and the Geant4 simulation.

2 Phoswich detector cell

The first flight model phoswich detector cell (PDC) has been used as the Compton scatterer in the present beam test. We note the energy deposited at the Compton site by the recoil electron is much lower than that at the photo-absorption site and hence detection of the electron signal in the fast scintillator poses a challenge.

Figure 2 shows a schematic view of the PDC and photographs of the components. The fast and slow plastic scintillators were produced by Eljen Technology in Texas, USA (EJ-204 and EJ-240, respectively). The BGO scintillators were provided by The Nikolaev Institute of Inorganic Chemistry in Novosibirsk, Russia. The fast and slow scintillators were wrapped in VM2000 sheets manufactured by 3M. The same reflective sheet was inserted inside the slow scintillator well to reflect back fast scintillator light yield. The slow scintillator was then wrapped with a thin tin foil and a thin lead foil (50 μm thick). These foils provide passive collimation for gamma-rays. The BGO scintillator was coated with a reflective layer of $BaSO_4$. The entire assembly was covered by a shrink tube to secure the metal foils and reflective sheets in place. The PDC was attached to Hamamatsu Photonics R7899EGKNP PMT assembly with silicone rubber. The same PMT same assembly will be used in the PoGOLite flight model. The assembly has a built-in power supply and provides stable high voltage (HV) within modest power consumption of about 300 mW/unit [32]. The HV ripple is ~ 0.05 photoelectrons level at a gain of 10^6.

The PMT signals from the last dynode were used for pulse shape discrimination of the fast scintillator hits from those in the slow scintillator and the BGO. In the present test, the signals were fed to a charge-sensitive amplifier (CSA, Clear Pulse 557), with a fanned-out output. The output of CSA was fed into two kinds of shaping amplifiers which had different time constants, 50 ns ('fast amp', Clear Pulse 4056) and 1 μs ('slow amp', Clear Pulse 4066). Since the fluorescent decay times of the BGO ($\sim$ 300 ns) and the slow scintillator ($\sim$ 230 ns) were longer than the time constant of the fast amp, only the first portion of the charge was integrated for the BGO and slow scintillators, while the fast scintillator signal was fully integrated by the fast amp. On the other hand in the slow amp, almost all of the charge was integrated for all scintillators. Therefore for the slow signals, the ratio of the fast shaping output to the slow shaping output was smaller than that for the fast signals. The PSD for a PDC was tested with a ^{241}Am source prior the beam test. The output pulse shape of the fast and slow shaping amplifiers corresponding to a 59.5 keV gamma-ray signal from a ^{241}Am source are shown in Fig. 3. As expected, the ratio of the fast to the slow amp outputs are significantly different. This is referred to as a double integration method of PSD [13–15,20–26].

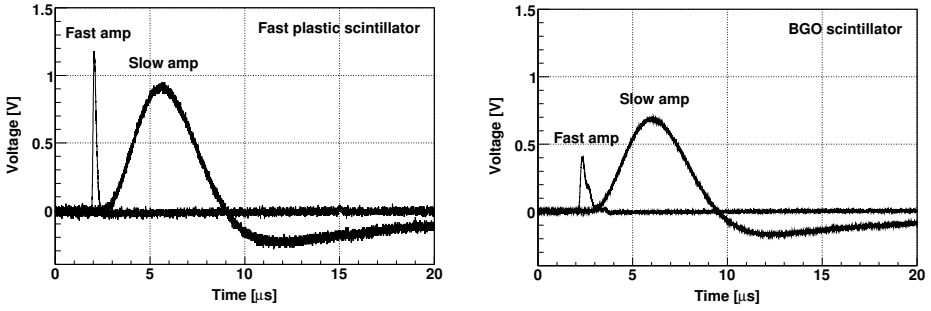

Fig. 3. The output pulse shape of the fast and slow shaping amplifiers for the 59.5 keV photoelectric absorption signal from the fast scintillator (left) and the BGO scintillator (right). The ratio of the fast shaping output voltage to the slow shaping output voltage is different.

The possible effect of charged cosmic-ray hits in the slow scintillator and BGO crystal on the fast scintillator signal was tested by measuring the ^{241}Am spectrum in the fast scintillator while the slow or BGO scintillator was irradiated with a ^{90}Sr β-ray source. Signal events (gamma-rays from ^{241}Am) were selected by comparing the output voltage of the fast and slow amplifiers (Fig. 4 and 5 left). Clean hits on the fast scintillator enter the dashed region: They are clearly separated from hits in the slow/BGO scintillator (background events). Projections of the two dimensional distributions of all events and selected fast events onto the vertical axis are given in Fig. 4 and 5 for data taking with ^{90}Sr on the slow scintillator and the bottom BGO respectively. The ^{241}Am spectrum including the photoelectric peak at 59.5 keV is recovered with no significant distortion. To evaluate possible effect charged particle cosmic-ray makes, the FWHM resolution for the photoelectric peak was calculated. The result was, 44±1% and 42±1%, obtained for the slow-irradiated and the BGO-irradiated data, respectively while the FWHM resolution was $42 \pm 1\%$ without ^{90}Sr. The spectra obtained by these three kinds of setups are summarized in Fig. 6. We conclude that background rejection using the phoswich technique reduces background efficiently without distorting the signal spectrum.

3 Beam test results

The prototype PoGOLite detector used in the test is constructed with 7 units, with one flight model PDC at the center. This was tested at KEK-PF during December 5−12, 2005.

During this experiment, backgrounds were not created artificially. Thus the slow and BGO scintillators were used to only reduce environmental radiation events. Polarization measurement under a high background, which may be made by radioactive sources, is scheduled at the next time at KEK-PF.

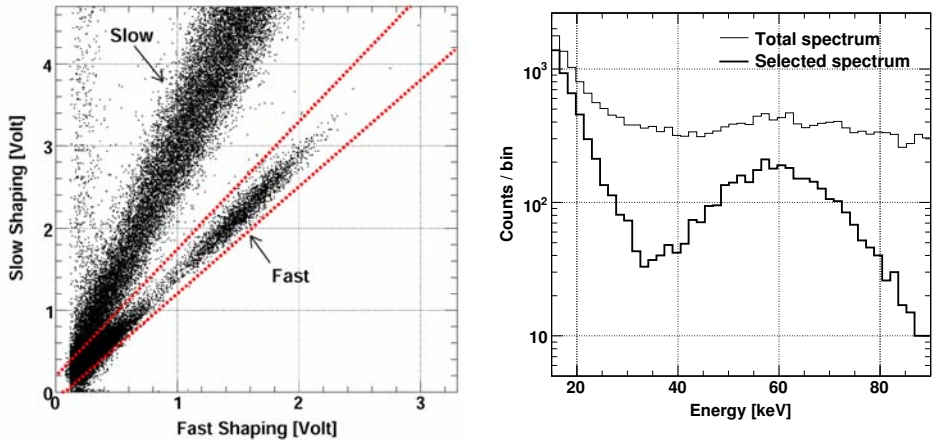

Fig. 4. Left: the relationship between the output of fast shaping amplifier and the slow shaping amplifier when the slow scintillator was irradiated by a ^{90}Sr source. The events surrounded by dashed lines are from the fast scintillator ('fast branch'). Right: total (thin line) and selected (thick line) spectra. The photoelectric peak at 59.5 keV appears clearly after the selection.

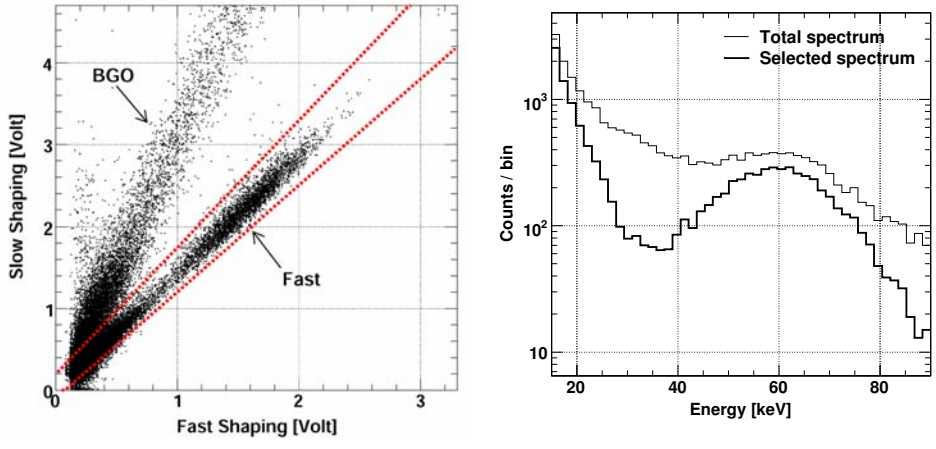

Fig. 5. Same for Fig. 4, but with the BGO scintillator irradiated by a ^{90}Sr source.

3.1 Setup and data taking

The prototype detector in the present test is shown in Fig. 7. The center unit is the first flight model PDC and the surrounding 6 units are made of the fast plastic scintillator rods of the flight model design but do not have the slow plastic scintillator well nor the bottom BGO. BGO crystals were substituted with acrylic light guides. The fast scintillators of the surrounding 6 units were wrapped with VM2000 and the light guides were covered by polytetrafluoroethylene tape. Each unit was attached to a Hamamatsu R7899EGKNP PMT assembly.

The experiment was carried out at station A of beam line 14 (BL14A). The

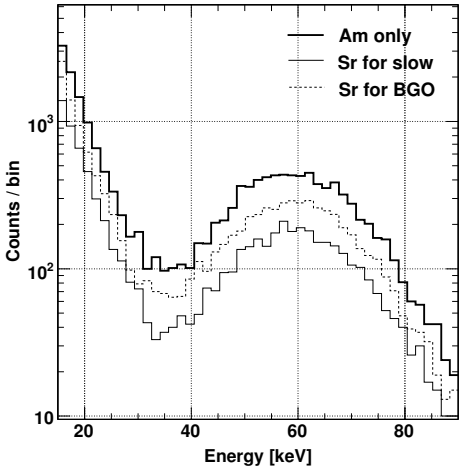

Fig. 6. Three spectra obtained with the background free setups (Am only), ^{90}Sr background irradiating the slow scintillator (Sr for slow) and ^{90}Sr background irradiating the BGO scintillator (Sr for BGO). The count rates are different due to dead time.

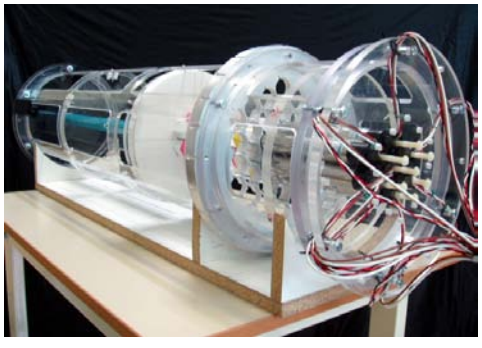

Fig. 7. A photograph of the PoGOLite prototype detector used in the December 2005 KEK-PF experiment.

Fig. 8. A photograph of the setup in the BL14A experimental hutch at KEK-PF. The instrument covered with a black sheet is attached to the experiment table on the right-hand side.

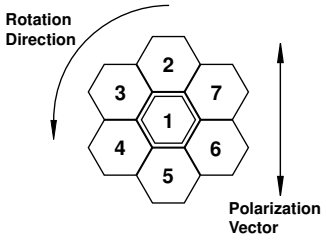

Fig. 9. The layout and numbering scheme of the prototype detector array at 0°, viewed from the beam origin. The central one (Ch.1) is the PDC unit.

setup is shown in Fig. 8. The BL14A can deliver a vertically plane-polarized beam via two monochromator Si(553) crystals between 30 keV and 80 keV. Data were taken at beam energies of 30, 50 and 70 keV. Although the detectable energy of PoGOLite goes down to 25 keV, we could not take a data of 25 keV. The intensity of the beam was reduced ~ 5000 times with metal attenuators made of tungsten and lead in order to prevent pile-up. The beam was collimated to a cross-sectional size of 1 mm squared by thick tantalum plates. The central PDC unit of the detector array was irradiated, and thereby acted as an active scatterer with the six peripheral units absorbing the scattered photons. The numbering scheme of the units and orientation of the polarization plane ('0 degree') are shown in Fig. 9. The instrument was rotated around the center of Ch.1 at 15° steps in the anti-clockwise direction covering the whole azimuthal angle. The count rates measured in each peripheral unit were modulated depending on the rotation angle. Since photons tend to be scattered in the direction perpendicular to the polarization vector, the count rates of Ch.2 and Ch.5 are predicted to be minimum at 0° and 180° and to be maximum at 90° and 270°.

The data acquisition (DAQ) system used in the beam test is shown in Fig. 10. The signals from the PMT anodes were used to trigger the DAQ. They were first amplified by a factor of 10 with current amplifiers. The outputs of the amplifiers were fed into the discriminators. Their threshold levels were about 0.3 photoelectrons and the width of the output signal was 50 ns. The outputs of discriminators were fed into a linear fan-in module and a discriminator (N.I.M. standard) to allow a hardware coincidence to be formed. The discriminator threshold voltage was set to -1 V. When at least two sensors fired, a DAQ cycle was initiated. Using this system, the coincidence of any combination of the units could be studied. The output from the last discriminator was widened (and delayed) with gate generators ('G.G.' in Fig. 10), and fed into a digital I/O board (Clear Pulse 2610) which acted as an interrupt register, and into the gate or sample hold (S/H) inputs of the ADC boards (Clear Pulse 1113A, peak hold type). When a signal is sent to the interrupt register, a Linux computer started to read out the ADCs via a VME bus, and a veto signal for the discriminators was asserted. The veto signal was cleared when DAQ cycle ended. The dead time was monitored by a 1 MHz clock and a scaler

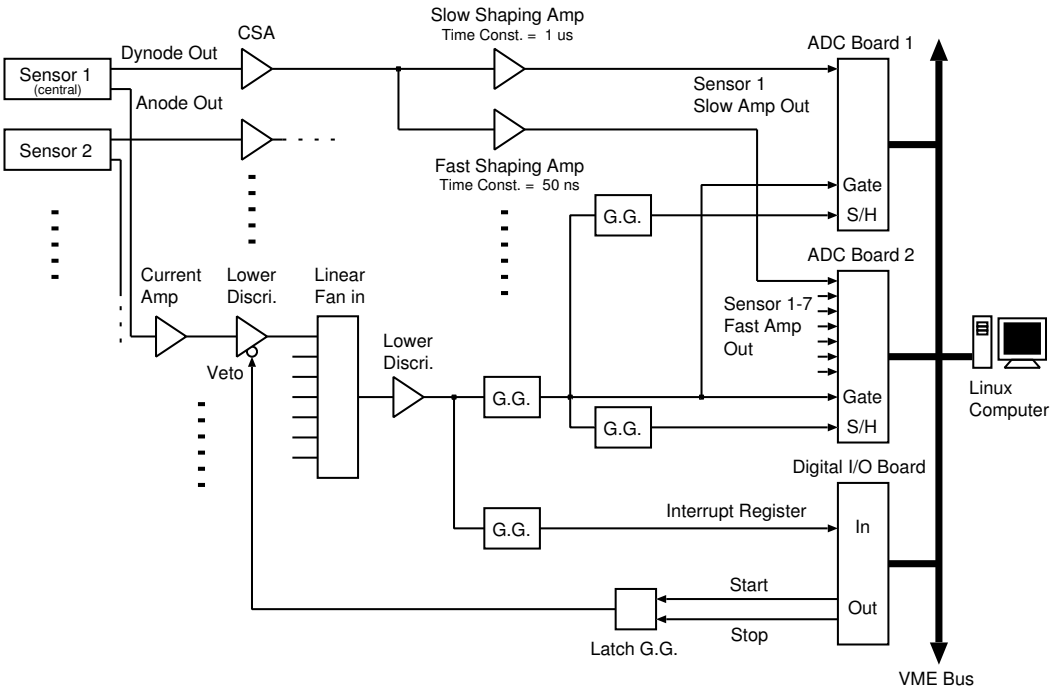

Fig. 10. The data acquisition system of the experiment. 'G.G.' means a gate generator and 'S/H' means a sample hold input.

and used to correct the count rates off-line. The dead time per event was about 130 μs. The PMT signals from the last dynodes were used for spectroscopy. The analog system used for the PDC in this experiment was same as for the experiment described in section 2. For the peripheral 6 units, we installed only fast shaping amplifiers.

Knowledge of the number of incident photons is needed to estimate the detection efficiency. Since we could not attach another detector due to space constraints in the beam line, the beam intensity was estimated by the photo-absorption rate at Ch.1. Therefore, a 10 minute run with Ch.1 trigger was inserted before each coincidence trigger run at an azimuth angle. The setup of Ch.1 trigger was realized by skipping the linear fan in and the subsequent discriminator. The number of incident photons was estimated by a combination of the simulation and the photo-absorption rate at Ch.1 (see §3.3). The background data were obtained after the 345°-run for each beam energy, once per a full azimuth rotation.

The polarization degree of the beam is essential in evaluating detector modulation factor. We used a polarization monitor consisted of a small cylindrical plastic scintillator (2.5 cm ϕ and 2 cm thick) glued to a PMT (Hamamatsu R7899EGKNP) and a small CdTe detector ($1.8 \times 2.0 \times 2.0$ mm crystal, Clear Pulse 181820). The monitor is shown in Fig. 11. The plastic scintillator and the CdTe detector were mounted on a turntable. The rotation axis of the table was aligned with the beam axis. The plastic scintillator was placed at the cen-

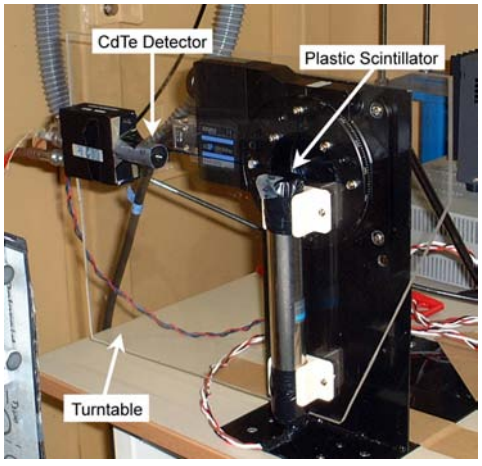

Fig. 11. A photograph of the calibration polarimeter. To shorten measurement time, the CdTe detector was closer to the plastic scintillator (4 cm away) during the measurement.

ter of the table, and the CdTe detector was placed 4 cm away from the plastic scintillator. When the table was rotated, the CdTe detector moved around the plastic scintillator scatterer in an azimuthal range of 180°. We have simulated the modulation factor for the polarization monitor with Geant4 and 90 % for the full polarization was derived. The beam polarization was measured to be 0.91 ± 0.01, 0.92 ± 0.01 and 0.91 ± 0.01 for 30, 50 and 70 keV, respectively.

3.2 Data analysis

Selection of clean events hitting the fast scintillator was done on the two-dimensional distribution of the two pulse-heights, one from the fast integrator and the other from the slow integrator. The two dimensional distribution for signals from Ch.1 taken in the 50 keV coincidence run is shown in the left panel of Fig. 12. Clean hits in the fast scintillator are separated from hits in the slow/BGO scintillator. The events with entries in the 'fast branch' (the dashed region in Fig. 12 left) include Compton-scattered events. Spectra for the unfiltered and filtered events are shown by thick and thin solid line, respectively in the right panel of Fig. 12. Events in the high energy range, corresponding to ambient background, were significantly reduced.

The energy was calibrated by using the 50 keV photoelectric peak in the filtered events. The ADC pedestal were obtained using test pulses.

The second step of data analysis is to select events with a photo-absorption site and a Compton scattering site. In the present setup, the Compton scattering site is Ch.1. This selection is done by examining the energy deposits in Ch.1 (E_1) and the sum of the energy deposit in Ch.1 and the photo-absorption site, one of Ch.2−7 ($E_{\rm tot}$). Distribution of the two energies for coincidence events

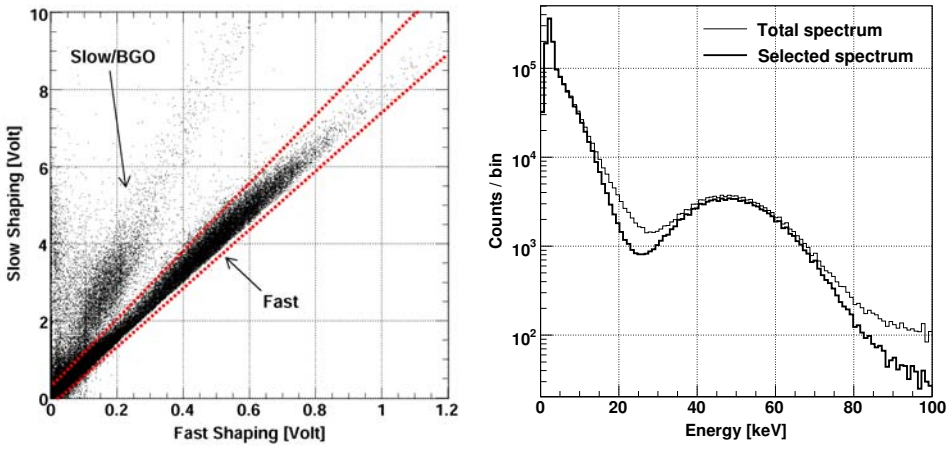

Fig. 12. Left: relation between the output of fast shaping amplifier and that of slow shaping amplifier for Ch.1 taken in the 50 keV coincidence run. Right: total (thin line) and selected (thick line) spectra for the 50 keV beam. Events in the high energy range, which were room background and cosmic-rays, were significantly reduced after the selection. Saturated in the slow shaping, these events do not appear in the left-hand figure.

are shown in the left panels of Fig. 13−15.

The region surrounded by the dashed line contains events where incident gamma-rays were scattered in Ch.1 and photo-absorbed in Ch.2−7, 'valid Compton scattering events.' The coincidence condition was applied as a part of off-line data analysis: the selection criteria were set to maximize the number of Compton scattering events, while reducing background events (photo-absorption in Ch.1, accidental coincidence between the beam and the room background). The criteria were:

- 30 keV run: 1 keV $\leq E_1 \leq$ 12 keV, 15 keV $\leq E_{\rm tot} \leq$ 55 keV and $E_{\rm tot} \geq 1.65E_1$.
- 50 keV run: 1 keV $\leq E_1 \leq$ 25 keV, 30 keV $\leq E_{\rm tot} \leq$ 80 keV and $E_{\rm tot} \geq 1.65E_1$.
- 70 keV run: 1 keV $\leq E_1 \leq$ 35 keV, 45 keV $\leq E_{\rm tot} \leq$ 100 keV and $E_{\rm tot} \geq 1.65E_1$.

This procedure corresponds to Compton kinematics filtering. The same criteria were applied to the background runs and the background were subtracted from the beam data, after the dead time correction. The background events accounted for $\sim 5\%$ for 30 and 50 keV and $\sim 15\%$ for 70 keV.

The numbers of signal events for each coincidence combination for 3 coplanar pairs, Ch.2 and Ch.5, Ch.3 and Ch.6 and Ch.4 and Ch.7 were plotted as a function of azimuthal angle settings in the right panels of the Fig. 13−15. The curves show the best-fit cosine functions.

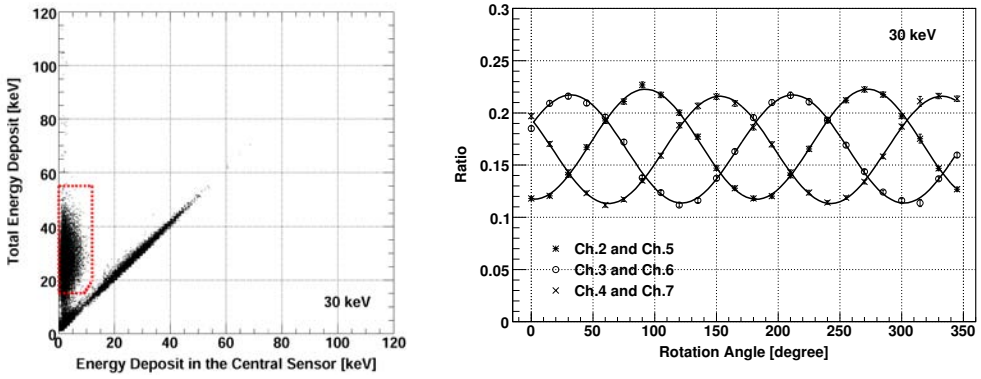

Fig. 13. Left: relation between energy deposit in the central sensor and the sum of the energy deposit in Ch.1 and in one of Ch.2−7 for the 30 keV beam. Right: modulation of the rates as the function of the rotation angle for the 30 keV beam.

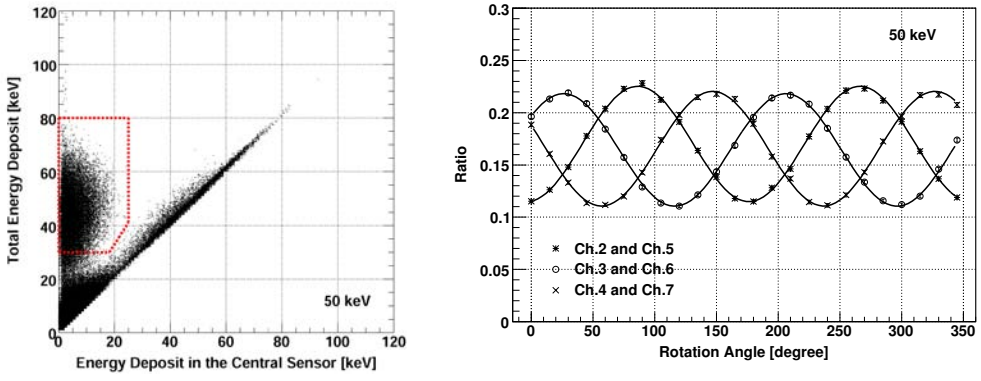

Fig. 14. Same as Fig. 13, but for the 50 keV beam.

The modulation factor, $M_{\rm obs}$, is defined on the maximum and the minimum ratios ($R_{\rm max}$ and $R_{\rm min}$, respectively) as,

$$M_{\rm obs} = \frac{R_{\rm max} - R_{\rm min}}{R_{\rm max} + R_{\rm min}}.$$

The expected modulation factor for 100% polarized gamma-rays, M_{100}, is defined as $M_{100} = M_{\rm obs}/P$, where P is the degree of polarization of the beam. We obtained M_{100} to be 0.344 ± 0.004, 0.358 ± 0.012 and 0.372 ± 0.011 for 30, 50 and 70 keV, respectively. [1] These results clearly show that polarization can be determined using the flight model PDC.

[1] The same Compton kinematics filtering described above was applied for the datasets acquired with the Ch.1 single trigger. Modulation factors were obtained as 0.346 ± 0.008, 0.360 ± 0.008 and 0.380 ± 0.009 for 30, 50 and 70 keV, respectively. They were consistent with the results of the coincidence trigger run.

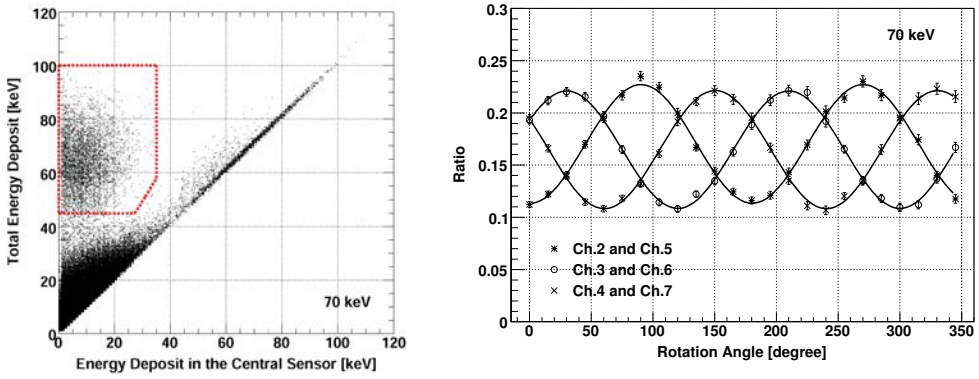

Fig. 15. Same as Fig. 13, but for the 70 keV beam.

3.3 Comparison with simulation

In this section, the experimental results are compared to simulated data. The simulation was performed with using the Geant4 Monte Carlo package. The treatment of the polarization vector of the Compton/Rayleigh scattered photons was modified [31]. The number of incident photons was 10^6 at each rotation angle. The results from the simulation are given in Table 1, together with the corresponding measurement at various energy bands. These results agree with the experimental results to an accuracy of $\sim 10\%$.

Detection efficiencies were calculated. The total number of the incident photons in the experiment, N_0, are estimated by $N_0 = N_{\rm abs}/p$, where $N_{\rm abs}$ is the number of the photo-absorption events in Ch.1 corrected with dead time, and p is the simulated fraction that photo-absorption occurs in Ch.1. The detection efficiency is defined by the total number of the 'valid Compton scattering events' divided by N_0. The resulting values are given in Table 1. The detection efficiencies agree within 10% between the experiment and the simulation. Fig. 16 shows the energy dependence of the detection efficiency derived from the experiment and the simulation.

The small differences between experiment and simulation for both of the modulation factors and the detection efficiencies could be due to the misalignment, uncertainties in the background subtraction, the uncertainty of the simulation and the complex light output response of the plastic scintillator (quenching effect, position dependency and so on).

We conclude the Geant4 simulation with our modification [31] reproduced the experimental modulation factor and the detection efficiency within $\sim 10\%$ (relative). The prototype phoswich polarimeter performs in line with the expectations derived from the Geant4 simulation. Some differences remained, however, and will be the subject of further careful examination.

Table 1
The comparison of the experimental results to the simulated values of the modulation factor and the detection efficiency. Errors include both statistical and systematic errors.

Energy [keV]	Modulation factor		Detection efficiency [%]	
	experiment	simulation	experiment	simulation
30	0.344 ± 0.004	0.388 ± 0.003	3.69 ± 0.12	3.974 ± 0.005
50	0.358 ± 0.012	0.403 ± 0.005	2.86 ± 0.07	2.610 ± 0.004
70	0.372 ± 0.011	0.409 ± 0.009	1.38 ± 0.09	1.341 ± 0.002

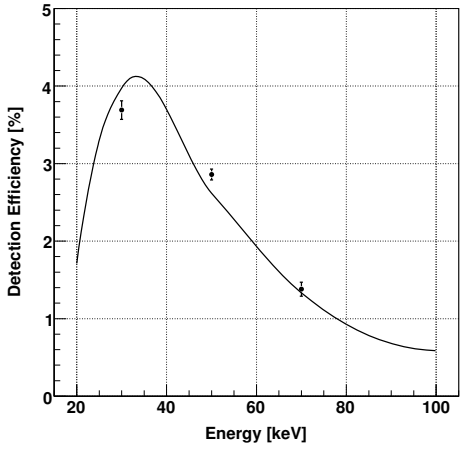

Fig. 16. Energy dependence of detection efficiency for the prototype model used in this experiment. The dots show the experimental value, while the line is the result of the simulation.

4 Summary

In this work, the performance of a complete phoswich detector cell (PDC) and a 7-unit prototype detector array including a PDC, have been studied for the PoGOLite astronomical soft gamma-ray polarimeter. The energy spectra of a ^{241}Am source with and without β-ray background from a ^{90}Sr source have been measured. A clear separation of the fast and the slow signal was obtained. After the pulse shape discrimination, the resolutions of the 59.5 keV photo-absorption peak were consistent, which demonstrated that the phoswich technique reduced background efficiently. In order to measure modulation factor and detection efficiency of the prototype including a flight model PDC and to compare the polarimeter's performance to a Monte Carlo simulation, a beam test was performed at BL14A in KEK-PF. The central PDC was irradiated by a highly polarized photon beam. The energy of the beam was 30, 50 and 70 keV. A polarization signal was clearly identified. The experimental result of the instrument modulation factors were compared to those derived from a simulation using the Geant4 package. They agreed with the results

of the simulation within $\sim 10\%$ accuracy. The detection efficiency of Compton scattered events was also determined. These values were reproduced by the simulation to < 10 %. These results confirm that the prototype phoswich polarimeter design adopted by PoGOLite performs in line with expectations from simulations.

Acknowledgments

We greatly appreciate the referees for their detailed comments which have improved this paper. We would also like to thank K. Hayashida for support for the experiment and valuable discussions. This work has been performed under the approval of the Photon Factory Program Advisory Committee (Proposal No.2005G023). We appreciate the generous and friendly support of the KEK-PF staff. This work is partially supported by Grant-in-Aid for Science Research (KAKENHI) 16340055, Japan Society for the Promotion of Science (JSPS); by Kavli Institute for Particle Astrophysics and Cosmology, Stanford University; and by the Knut and Alice Wallenberg Foundation and The Swedish National Space Board. M.U. is supported by JSPS Research Fellowship for Young Scientists.

References

[1] F. Lei, et al., Space Sci. Rev. 82 (1997) 309.

[2] M.C. Weisskopf, et al., Astrophys. J. 208 (1976) L125.

[3] M.C. Weisskopf, et al., Astrophys. J. 220 (1978) L117.

[4] E.H. Silver, et al., Astrophys. J. 225 (1978) 221.

[5] K.S. Long, et al., Astrophys. J. 238 (1980) 710.

[6] W. Coburn and S. Boggs, Nature 423 (2003) 415.

[7] R.E. Rutledge and D.B. Fox, Mon. Not. Roy. Astron. Soc. 350 (2004) 1272.

[8] C. Wigger, et al., Astrophys. J. 613 (2004) 1088.

[9] N. Produit, et al., Nucl. Inst. and Meth. A 550 (2005) 616.

[10] J. Legere, et al., Proc. SPIE 5898 (2005) 413.

[11] S. Gunji, et al., Proc. ICRC (2003) 2779.

[12] R. Silva, et al., Proc. SPIE 4843 (2003) 543.

[13] T. Kamae, et al., Proc. SPIE 1734 (1992) 2.

[14] T. Kamae, et al., IEEE Trans. Nucl. Sci. NS-40 (2) (1993) 204.

[15] T. Takahashi, et al., IEEE Trans. Nucl. Sci. NS-40 (4) (1993) 890.

[16] S. Gunji, et al., Astrophys. J. 397 (1992) L83.

[17] S. Gunji, et al., Astrophys. J. 428 (1994) 284.

[18] S. Miyazaki, et al., Pub. Astron. Soc. Japan 48 (1996) 801.

[19] N. Yamasaki, et al., Astrophys. J. 481 (1997) 821.

[20] T. Kamae, et al., Proc. SPIE 2806 (1996) 314.

[21] T. Takahashi, et al., Astronomy Astrophys. Suppl. 120 (1996) 645.

[22] J. Kataoka, et al., Proc. SPIE 3445 (1998) 143.

[23] K. Makishima, et al., in: H. Inoue, H. Kunieda (Eds.), A.S.P Conf. Proc. 251, Astr. Soc. of Pacific (2001) 564.

[24] M. Kokubun, et al., IEEE Trans. Nucl. Sci. NS-51 (2004) 1991.

[25] T. Takahashi, et al., Pub. Astron. Soc. Japan, submitted for publication.

[26] M. Kokubun, et al., Pub. Astron. Soc. Japan, submitted for publication.

[27] P. Chen, et al., Proc. IEEE Nucl. Sci. Symp., Portland, OR, October 2003.

[28] S. Larsson and M. Pearce, Nucl. Inst. and Meth. A 525 (2004) 148.

[29] K. Gunderson, et al., Proc. SPIE 5165 (2004) 158.

[30] T. Mizuno, et al., Astrophys. J. 614 (2004) 1113.

[31] T. Mizuno, et al., Nucl. Inst. and Meth. A 540 (2005) 158.

[32] J. Kataoka, et al., Proc. SPIE 5898 (2005) 133.